

STRUKTURA 2022

Tábor, 20. 6. - 23. 6. 2022

Session I, Monday, June 20

L1

FIRST FIFTY YEARS OF POWDER DIFFRACTION: FROM PAUL SCHERRER TO HUGO RIETVELD

F. Laufek

Czech Geological Survey, Geologická 6, 152 00 Praha 5, Czech Republic
frantisek.laufek@geology.cz

In 1912, Max von Laue, Walter Friedrich, and Paul Knipping performed their famous X-ray diffraction experiment and proved for the first time two basic principles in physics: that a single crystal is composed of regular blocks and that X-rays behave as waves with a wavelength in the order of the distances between the building blocks of the crystal. It is interesting to note, that Friedrich and Knipping also carried out first powder X-ray diffraction experiment. They ground a copper sulphate crystal and placed the powder sample in the X-ray beam instead of a single-crystal. They observed small speckles around a central spot. Unfortunately, they used a polychromatic beam and the exposure was too short to observe diffraction rings [1].

The powder X-ray diffraction method was developed independently by Peter Debye and Paul Scherrer (1916) and by Alfred Hull (1917). Debye and Scherrer made a 57 mm diameter cylindrical camera, used two films with each forming two half of circle in contact with a camera wall, a primary beam collimator and a light-tight cover. For the sample, they used the finest grain powder of LiF [2]. Debye and Scherrer were surprised to find on the first photographs the sharp lines of first powder diagram, which they correctly interpreted as crystalline diffraction by the randomly oriented micro-crystal of the powder [3]. Approximately at the same time, Alfred Wallace Hull, an employee of General Electric Research Laboratory in USA, became interested in the X-ray diffraction. Hull saw there a challenge and try to find the crystal structure of iron. Since the single-crystals of iron were not available at that time, he used iron fillings, which were rotated continuously in order to provide randomness [3]. He obtained good diffraction patterns and subsequently checked if the d -spacings of the diffraction patterns of iron are consistent to the Bragg values for the three cubic crystal systems [1]. Hull also described

many of the experimental factors; was first who used a K filter and measured the effect of X-ray voltage on the intensity of the $MoK\alpha$ radiation. He described the importance of the particle size in the sample, specimen rotation and the necessity for the random orientation. Debye and Scherrer did not mention the use of the method for phase identification in the paper (1916), however Hull recognized that powder diffraction analysis can be used for phase identification of crystalline compounds, even if they are in mixtures. A major advance of the powder diffraction method began in the early 1950's with the introduction of the first commercial high-resolution diffractometers which greatly expand the use of the method [3]. In 1967, a next huge step was taken as Hugo Rietveld published his first whole profile pattern fitting analysis of WO_3 [4]. In this work, Hugo Rietveld showed that he could refine a crystal structure having powder diffraction pattern with overlapping reflections. He also introduced residual values (R factors), allowing the quantitative judgment of the refinement quality.

This contribution illustrates the discovery of powder diffraction in 1916 and further development of the method till the advent of „Rietveld method“ in 1967. The progress in development of instrumentation (including neutron diffraction), powder diffraction databases, and determination of first non-cubic crystal structures will be discussed.

1. M. Etter, R.E. Dinnebier, *Z. Anorg. Allg. Chem.*, 640, (2014), 3015.
2. A. Authier, *Early Days of Crystallography*, IUCr, Oxford University Press, Oxford, 2015.
3. W. Parrish, J.I. Langford, Powder and related techniques: X-ray techniques, *International Tables for Crystallography*, volume C, IUCr London, 1999.
4. H. M. Rietveld, *Acta Crystallogr.* **22**, (1967), 151.



L2

EXPERIENCES WITH PARTICIPATION IN CRYSTAL STRUCTURE PREDICTION TEST - CSP7

M. Hušák, F. Fňukal

University of Chemistry and Technology, Prague, Technická 5, 166 28 Praha 6 – Dejvice
husakm@vscht.cz

Introduction

Blind crystal structure prediction (CSP) test is a periodic event organized by Cambridge Crystallographic Data Centre. Structure prediction typically consists from 3 phases:

- 1) Building a 3D molecule model from its connectivity information
- 2) Generating a set of suggested structures
- 3) Ranking of the suggested structures

This year, it was optional to participate only in the phase 3). We had participated in ranking of suggested structures of following molecules:

Methods

Based on preliminary benchmarks we had used for the ranking energy calculation ground on DFT theory. We had used rSCAN functional combined with MBD dispersion correction. The data were prepared in BIOVIA Materials Studio software. Computation was performed on Karolina supercomputer at TU Ostrava. CASTEP 20.11 software was used. The computational power required for the calculations was approximately 2 000 000 core/hours.

Results

Based on the energy ranking, we had identified following structures from the input data sets as the one probably existing in reality: XXVII_structure_59, XXXI_structure_59, XXXIII_structure_452. The correct results of CSP7 were not disclosed up to now so we can not confirm any success.

During the data processing we were faced with limitation of commercial software used for CIF data transfer to DFT software acceptable format as well as with issues related to manage multiple jobs on a supercomputer. Based on the experiences we had chosen to develop our own software for DFT calculation handling.

Development of the CheckCIF-DFT code

The CheckCIF-DFT code is software targeted primary for transformation of CIF files to format acceptable by DFT software. The code just supports CASTEP and Quantum Espresso formats. The program can manage external DFT software run as well as analyze results. It can manage computation of multiple structures collection suitable for structure prediction. Calculation setup can be defined in a form of user-editable templates. The code was tested on structure ranking of the XXXI CSP7 target. Calculations on an 8 core PC (PBE functional with Grimme dispersion correction, Quantum Espresso) take 5 months. The results suggested the same structure (XXXI_structure_59) as the previous calculation. The code can be utilized for crystal structure solution verification, low-quality structure solution improvement as well as for light atom position clarification.

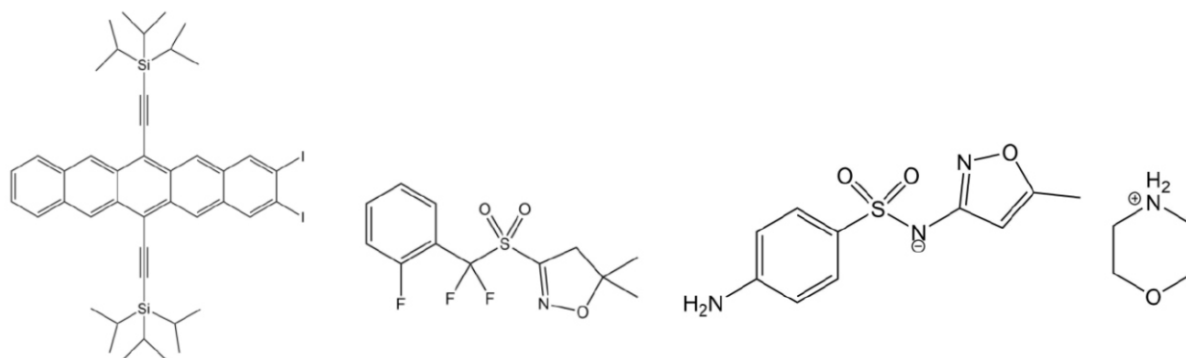


Figure 1. Structures from CSP7 test, XXVII (100 suggestions), XXXI (100 suggestions), XXXIII (500 suggestions)

STRUCTURE OF HALLOYSITE NANOTUBE WITH IRINOTECAN SOLVED BY MOLECULAR SIMULATION METHODS

M. Pospíšil¹, M. Pšenička¹, E. Gianni², D. Papoulis², K. Avgoustakis³

¹Charles University, Faculty of Mathematics and Physics, Prague, CZ

²Department of Geology, University of Patras, Rio, 26504, Patras, Greece

³Department of Pharmacy, University of Patras, Rio, 26504, Patras, Greece

miroslav.pospisil@mff.cuni.cz

Halloysite is a clay mineral derived from kaolinite with proven spiral-shape tubular crystal morphology and moreover biocompatible with the human body. It determines halloysite for possible use as drug delivery nanocarrier because it allows the encapsulation of various bioactive molecules. Halloysite nanotubes have been investigated as a potential drug delivery system of irinotecan for colon cancer treatment administered by the oral route [1]. To allow releasing of irinotecan in an intestinal environment the whole halloysite nanotubes loaded with irinotecan were coated with EudragitS100 to protect releasing of irinotecan in stomach pH. The loading efficiency of the halloysite nanotube for irinotecan was very high, reaching 84.42 ± 3.10 %. Experimental measurements like transmission electron microscopy showed that the irinotecan molecule is just on the surface of nanotubes and X-ray diffraction patterns proved that there was no intercalation of irinotecan among individual layers. Based on thermogravimetric analysis and tests with various weight ratios between halloysite and polymer was shown that drug release rate from the polymer-coated nanotubes was minimal (0.7 % in

2 h) at stomach pH (pH 1.2) and high at intestinal pH 7.4 conditions (when the pH was increased to 7.4, drug release increased by approx. 70 % in 2 h) [1]. Based on experimental results, methods of molecular simulations were used to determine mutual positions and arrangements of irinotecan molecules on the halloysite nanotube surface, which means the most probably structural model. Results of calculations showed that the most appropriate amount of irinotecan molecules for a given size of halloysite nanotube with a length of 25.359 Å is 6. This amount is in a good agreement with the molar weight ratio of the compounds determined from the real samples. Calculated models showed that the energetically preferred positions of the irinotecan molecules remain closed to the outer part of the halloysite nanotubes and longitudinal axes of irinotecan and the nanotube are parallel.

1. E. Gianni, K. Avgoustakis, M. Pšenička, M. Pospíšil, D. Papoulis, *Journal of Drug Delivery Science and Technology*, **52**, (2019), pp. 568-576.

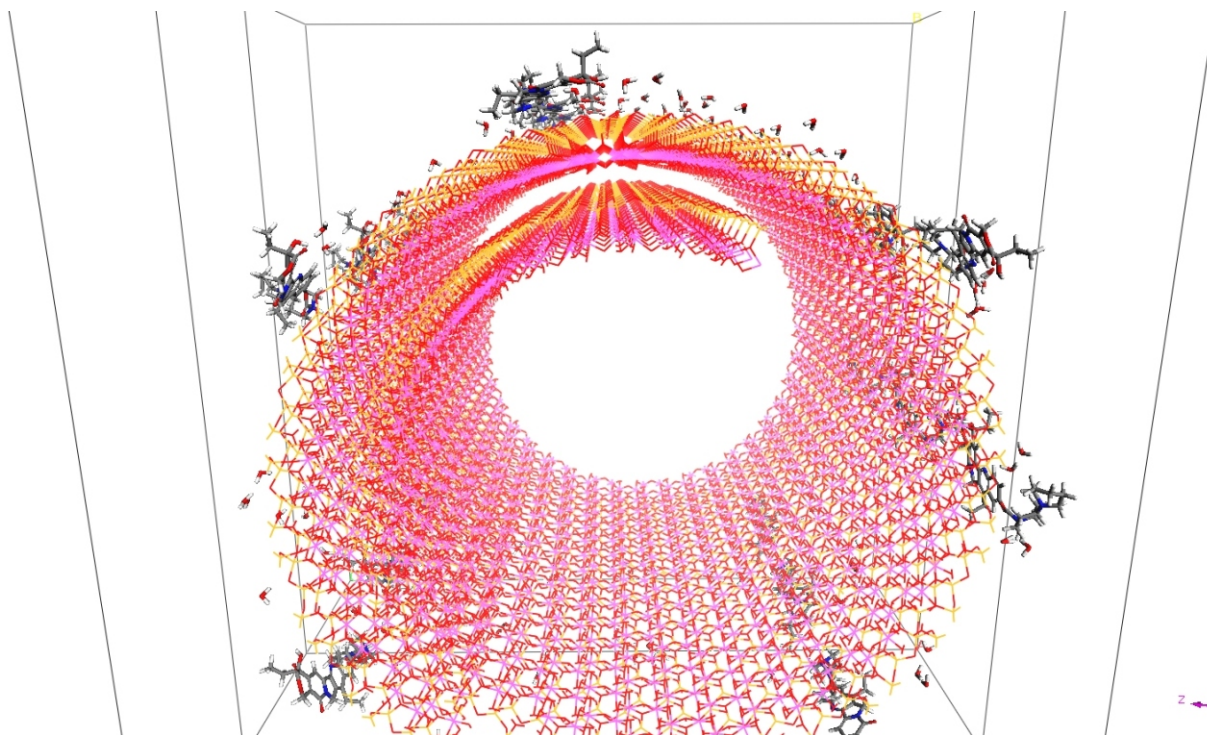


Figure 1. View along longitudinal axe for the optimized structure of the halloysite tube with 6 drug molecules.



L4

FIBRE TEXTURES OF CRONSTEDTITE

J. Hybler

*Institute of Physics, Czech Academy of Sciences, Na Slovance 2, 182 21 Praha 8, Czech Republic
hybler@fzu.cz*

Keywords: cronstedtite; 1:1 layer silicates; fibre textures

The layered 1:1 silicate cronstedtite ($\text{Fe}^{2+}_{3-x}\text{Fe}^{3+}_x(\text{Si}_{2-x}\text{Fe}^{3+}_x)\text{O}_5(\text{OH})_4$, $(0.5 < x < 0.85)$) belongs to the serpentine-kaoline group. It forms relatively numerous polytypes generated by stacking 1:1 structure building layers – equivalents of OD packets with the trigonal protocell $a = 5.5$, $c = 7.1$ Å. Polytypes are subdivided into four OD subfamilies, or Bailey's groups A, B, C, D according to different stacking rules. Cronstedtite occurs rarely in low temperature hydrothermal deposits [1], in certain meteorites (CM chondrites) [2], and presumably on asteroids. Synthetic micron-size crystals were prepared by Pignatelli and her co-workers [1,3].

The data collected by four circle single-crystal X-ray diffractometer with area detector processed by an appropriate software provide precession-like reciprocal space sections (RS sections in the following). Similar RS sections are obtained by electron diffraction tomography (EDT), for micron-size crystals [1]. Distributions of so called subfamily reflections along the reciprocal lattice rows $[2\bar{1}l]^* / [11l]^* / [\bar{1}2l]^*$ in $(2h\bar{h}l_{\text{hex}})^* / (hhl_{\text{hex}})^* / (\bar{h}2hl_{\text{hex}})^*$ RS planes is used for subfamily determination. Similarly, distributions of characteristic reflections along $[10l]^* / [01l]^* / [11l]^*$ rows in $(h0l_{\text{hex}})^* / (0kl_{\text{hex}})^* / (\bar{h}hl_{\text{hex}})^*$ planes allow determination of particular polytypes. For this purpose, graphical identification diagrams simulating distribution of reflections along named rows are used [1]. Modern diffractometers allow checking of many specimens and quick generation of RS sections. These techniques allow identification of various polytypes, twins, as well as allotwins – oriented crystal associations of more polytypes.

Lot of specimens of cronstedtite from various terrestrial localities and synthetic run products were studied by the author [1, 4, 5, 6]. RS sections were recorded, and selected ones were published and interpreted.

Recently cronstedtite from the new locality in Morocco was studied [6]. The sample was originally collected in 2017 by local people digging for mineral specimens from the hydrothermal veins with pyrite and calcite hosted in a skarn body situated at the base of the El Hammam hill (Djebel el Hammam), close to the Wadi (Ouedi) Beht (Beht river). It is located near the El Hammam fluorite deposit, ~45 km SW of Meknčs in the northeastern part of the Variscan Moroccan Central Massif in northern Morocco. The sample was purchased from Fabre Minerals by M. Števkó for the National Museum, Prague, where is now stored (catalogue No. PIN 114314).

The specimens separated from the sample provided a relatively high number of common as well as unusual (non-standard) polytypes of subfamilies A and D. Many crystals were identified as twins and/or allotwins of more polytypes (up to six). In many cases, the particular

polytypes were mechanically separated by cleaving of allotwinned crystals. Some polytypes found were not known to date [6].

Several specimens separated from the central part of the sample appeared to be polycrystalline aggregates with a strong fibre texture – (001) preferred orientation and azimuthally misoriented (100) and (010) directions of domains or crystallites. The $(2h\bar{h}l_{\text{hex}})^* / (hhl_{\text{hex}})^* / (\bar{h}2hl_{\text{hex}})^*$ and $(h0l_{\text{hex}})^* / (0kl_{\text{hex}})^* / (\bar{h}hl_{\text{hex}})^*$ RS sections indicating the subfamily D and $2H_2$ polytype were superimposed (Fig. 1a). In order to further examine this peculiar kind of intergrowths, the series of RS sections $(hk0_{\text{hex}})^*$, $(hk1_{\text{hex}})^*$, $(hk2_{\text{hex}})^*$, $(hk3_{\text{hex}})^*$, $(hk4_{\text{hex}})^*$, etc., perpendicular to \mathbf{c}_{hex} was generated. In these sections, concentric rings around \mathbf{c}_{hex} were recorded instead of discrete reflections. The apparent reflections visible in $(2h\bar{h}l_{\text{hex}})^* / (hhl_{\text{hex}})^* / (\bar{h}2hl_{\text{hex}})^*$ and $(h0l_{\text{hex}})^* / (0kl_{\text{hex}})^* / (\bar{h}hl_{\text{hex}})^*$ RS sections represented in fact intersections of named planes with these rings rather than discrete points. The nature of rings varied from sample to sample, from coarse-grained to quite smooth (Figs. 1b-d). However, in addition of $[00l]^*$ row with discrete maxima, some reflections and/or denser maxima on rings were usually present in the reciprocal space, so that indexing of diffraction patterns and generation of RS section became possible. For few crystals, however, the indexing procedure failed, possibly due to 'too perfect' rings in the reciprocal space.

The back-scattering electrons (BSE) photograph of one of these specimens revealed existence of domains elongated in the \mathbf{c} direction, probably azimuthally misoriented. (Fig. 2a). For comparison, a BSE image of an ordinary single crystal of the subfamily D is added (Fig. 2b). The electron microprobe analysis revealed partial substitution of Mn and Mg for Fe (0.09-0.10 and 0.19-0.25 a.p.f.u., respectively).

1. J. Hybler, M. Klementová, M. Jarošová, I. Pignatelli, R. Mosser-Ruck, S. Ďurovič, *Clay. Clay Miner.*, **66**, (2018), 379–402, DOI: 10.1346/CCMN.2018.064106.
2. I. Pignatelli, E. Mugnaioli, Y. Marrocchi, *Eur. J. Mineral.*, **30**, (2018), 349-354, DOI: 10.1127/ejm/2018/0030-2713.
3. I. Pignatelli, E. Mugnaioli, J. Hybler, R. Mosser-Ruck, M. Cathelineau, N. Michau, *Clay. Clay Miner.*, **61**, (2013), 277-289, DOI: 10.1346/CCMN.2013.0610408.
4. J. Hybler, J. Sejkora, V. Venclík, *Eur. J. Mineral.*, **28**, (2016), 765-775, DOI: 10.1127/ejm/2016/0028-2532
5. J. Hybler, *Eur. J. Mineral.*, **28**, (2016), 777-788, DOI: 10.1127/ejm/2016/0028-2541
6. J. Hybler, J. Sejkora, Z. Dolníček, M. Števkó, *Clay. Clay Miner.*, **69**, (2016), 702-734, DOI: 10.1007/s42860-021-00157-2

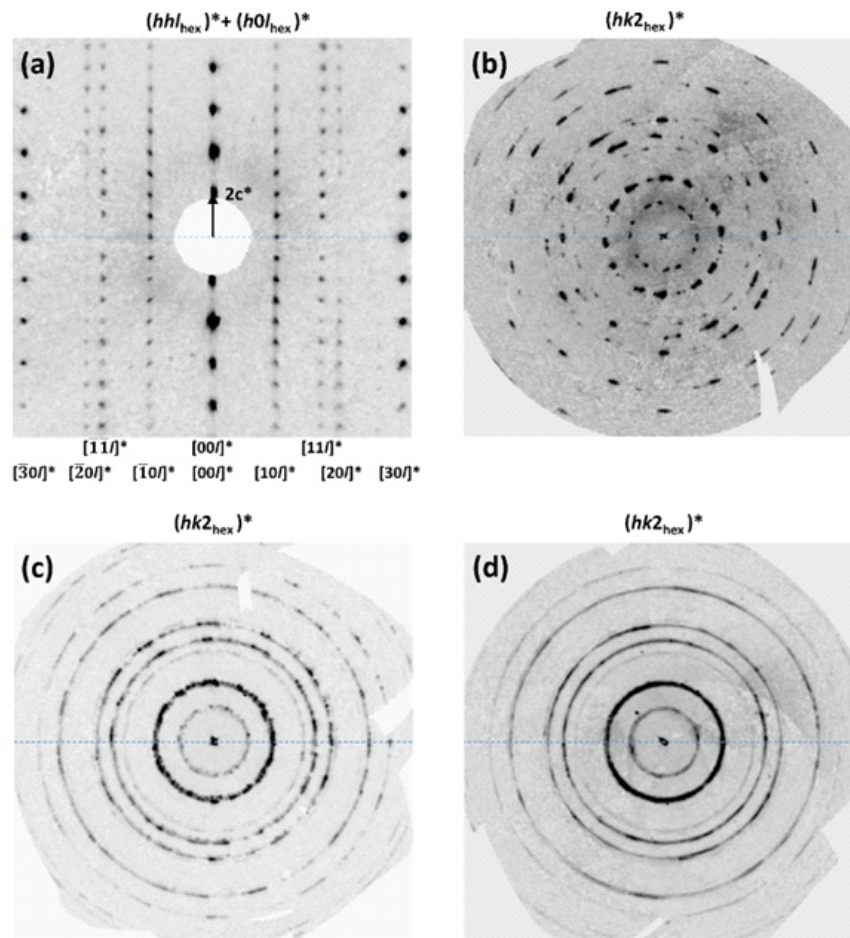


Figure 1. Examples of RS sections of strongly textured polycrystalline samples. **a** The apparent superposition of $(hhl_{hex})^*$ and $(h0l_{hex})^*$ sections of the well-ordered $2H_2$ polytype of the subfamily D. **b-d** Examples of diffraction rings at the level of $(hk2_{hex})^*$ RS section of several specimens varying from coarse-grained to almost smooth.

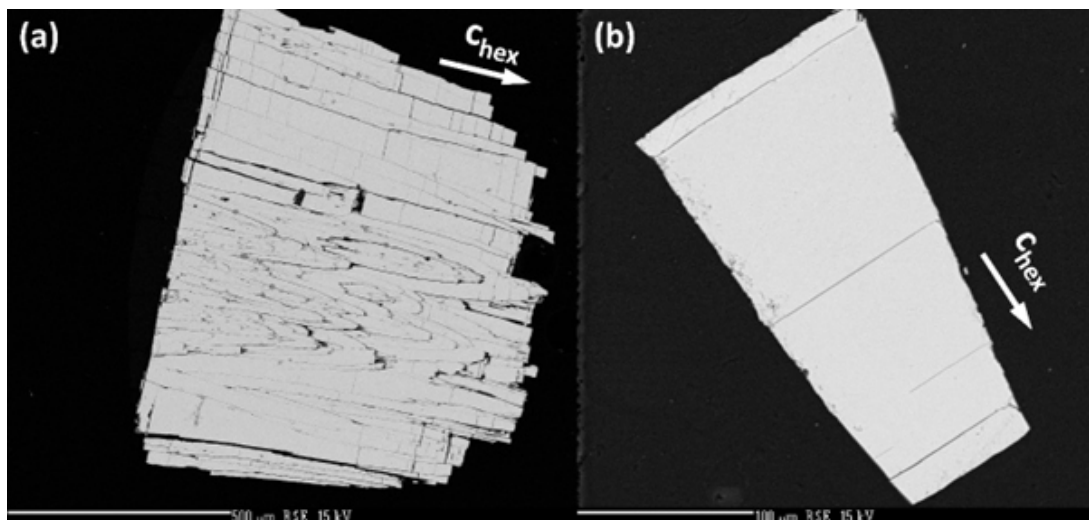


Figure 2. **a** The BSE image of the polycrystalline aggregate with fibre texture. Crystals are elongated about c_{hex} and are parallel to the section in clusters above and below the centre of the image. In the central cluster, the orientation of crystals is somewhat inclined, so that they are cut obliquely. Borders of individual crystals are recognizable. **b** The BSE image of the common single crystal of the subfamily D. Note the same degree of grey throughout the surfaces of both specimens due to the homogeneity of chemical composition. Photo Z. Dolníček.

The research was supported by project 18-10504S of the Czech Science Foundation, and by project CZ.02.1.01/0.0/0.0/16_019/0000760 Solid 21 under the Ministry of Educa-

tion, Youth and Sports. Author also thanks National Museum for allowing of taking of specimens for the study.



L5

“PŘÍRODNÍ SLITINY” Z HLUBOKOMOŘSKÝCH KONKRECÍ

J. Kopeček^{1,*}, F. Laufek², L. Klimša¹, A. Michalcová, L. Šulcová³, A. Tsepeleva³,
K. Borkovcová³, D. Nováček³, Hong N. Vu³, P. Dvořák³, P. Novák³

¹Department of Materials Analysis, Institute of Physics of the CAS, Prague, Czech Republic

²Czech Geological Survey, Prague, Czech Republic

³Department of Metals and Corrosion Engineering, University of Chemistry and Technology Prague, Prague, Czech Republic

*kopecek@fzu.cz

Kritický nedostatek barevných kovů spojený s tranzicí ekonomiky vede k hledání méně obvyklých zdrojů, jako jsou například hlubokomořské konkrece. Zatímco konvenční těžba je ekologicky závadná nebo probíhá v nedostatečně přátelských teritoriích, zóny hlubokomořského dna jsou volně dostupné nebo předmětem mezinárodních smluv, které je činí právně přístupné (např. společný claim několika post-socialistických zemí v zóně Clarion-Clipperton v Tichém oceánu). Odhlédneme-li od realizačních obtíží či vysokých vstupních nákladů, jedná se o zajímavý technologický i strukturální problém. Tradiční přístup ke konkrecím vycházel z postupné separace a následného čištění jednotlivých obsažených prvků a v hledání těch, které jsou finančně náležitě zajímavé pro těžbu. Projekt, jehož výsledky jsou prezentovány vychází z revoluční myšlenky „přírodních slitin“, tedy v redukci nikoli na čisté kovy, ale na čistou směs kovů, která bude následně využita jako funkční příměs například do hliníkové matrice. Konkrece byly redukovány aluminotermicky a titanotermicky se stechiometrickým a zvýšeným obsahem redukujícího kovu (obvykle 0, 10, 20 a 100 % přebytku).

Struktura takto získaných slitin byla následně studována strukturálně (kombinace XRD, LOM, SEM), mechanicky i korozně. Získané výsledky jsou překvapivě komplexní – struktura je složitá, pozorované fáze jsou nestechiometrické, případně jsou prvky ve strukturách substituovány. Slitina bez přebytku hliníku při aluminotermii obsahuje majoritní fázi - $Mn_{0,66}Ni_{0,2}Si_{0,16}$ a tři minoritní fáze; slitina s 10 % přebytku obsahuje sedm fází, z nichž tři mají přes 10 hm. %; slitina s 10 % přebytku obsahuje 9 fází,

z nichž pět je minoritních. Majoritní fáze ve všech vzorcích je odlišná. Mechanické vlastnosti jsou poplatné majoritnímu podílu manganu – připravené vzorky jsou tvrdé a extrémně křehké [1], avšak korozní vlastnosti jsou dobré [2]. Materiály připravené titanotermicky nechávají extrémní množství materiálu ve strusce, avšak výsledné složení není tak komplexní jako v případě aluminotermických materiálů. Ostatně výchozí fázové složení samotných konkrecí je také složité: obsahují birnessit, todorokit a křemen a další minoritní fáze.

Metodologicky byla práce postavena na součinnosti metod XRD (Bruker D8 Advance) a SEM (Tescan FERA 3) včetně analyzátorů EDS a EBSD (EDAX Octane Super 60 mm² a DigiView V). Bylo dosaženo dobré shody v obsahu fází stanovených pomocí XRD a EBSD/EDS. Některé zcela minoritní fáze byly potvrzeny pomocí EDS/EBSD, protože stejnou krystalografickou strukturu v materiálu mají i jiné, více zastoupené fáze (případ MnS). V aluminotermických slitinách byly potvrzeny Heuslerovy fáze Mn_2FeAl a Mn_2FeSi vlastně dříve než byl publikován jejich objev v čistých ternárních systémech.

1. Novák P, Nguyen H V, Šulcová L, Kopeček J, Laufek F, Tsepeleva A, Dvořák P, Michalcová A 2021, Materials 14 561.
2. Msallamová Š, Novák P, Miossec P, Kopeček J, Tsepeleva A, Rudomilová D, Fojt J 2021 Materials 14 5211.

Výzkum je podporován GA ČR z projektu 20-15217S a strukturálními projekty MŠMT CzechNanoLab (LM 2018110) a SOLID21 (CZ.02.1.01/0.0/0.0/16_019/0000760).

STRUCTURE AND MICROSTRUCTURE IN (111) AND (111)+(001) ScN/MgO THIN FILMS

E. de Prado, J. More Chevalier, S. Cichoň, L. Fekete, J. Lančok

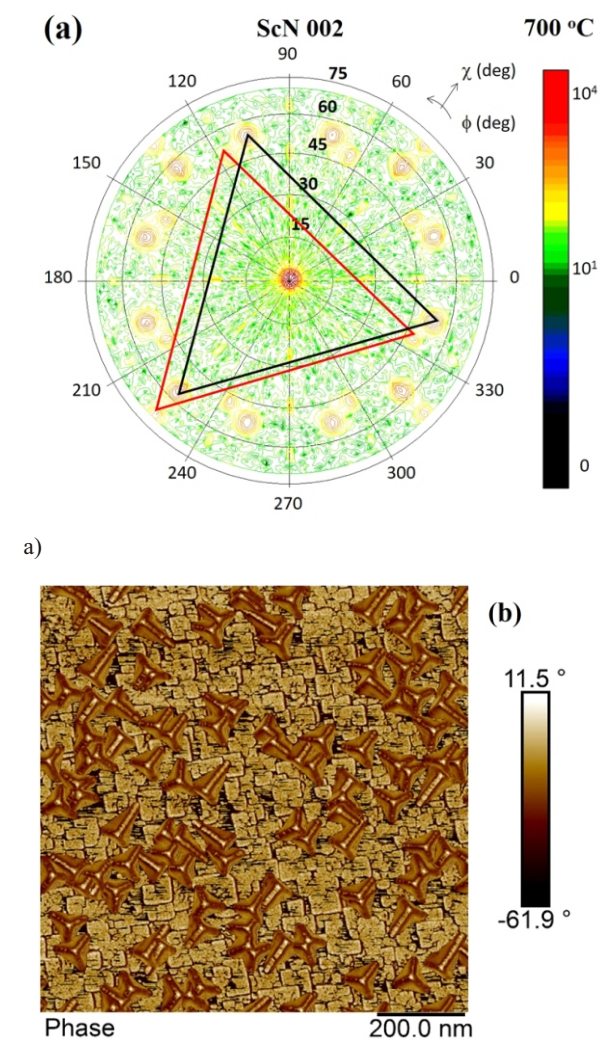
*Institute of Physics of the Czech Academy of Sciences, Na Slovance 2, 18221 Praha 8, Czechia
prado@fzu.cz*

ScN is an emerging semiconductor that exhibits rock-salt (cubic) crystalline structure. It is of high interest in material science due to its physical properties such as high melting point and high electron mobility. To improve the mobility and other electronic properties, it is necessary to produce single crystal ScN thin films with low density of defects. It has been demonstrated that the presence of point defects and impurities affects thermoelectric properties. Planar defects such as twins have been also explored for (111) and (001) ScN thin films grown on different substrates. The presence of twins for bi-oriented (111)+(001) ScN films on MgO (001) has been reported but its origin is not fully understood yet. In this work we pay special attention to the system (111)+(001) ScN/MgO (001) and we compare our results with single oriented (111) ScN films. To it, several ScN films were deposited on MgO (001) substrate by DC reactive magnetron sputtering at different temperatures. The morphology of the films has been explored by Atomic Force Microscopy (AFM) and the presence of twins has been analyzed by X-Ray Diffraction through 2 θ scans, and 002, 022, and 111 pole figures.

For the bi-oriented kind of films a very complex system of twins is obtained (Figure 1), which can be separated in the contribution of two, one coming from the (001) ScN oriented crystals and the other one coming from the (111) crystals. A deep study of the structure and microstructure of such a system could provide a better understanding of the role of twins in the final film orientation.

Keywords: ScN; twins; pole figure; epitaxial layer

1. M. A. Moram, T. B. Joyce, P. R. Chalker, Z. H. Barber, and C. J. Humphreys, "Microstructure of epitaxial scandium nitride films grown on silicon," *Appl. Surf. Sci.*, vol. 252, pp. 8385–8387, 2006.
2. S. Kerdsonpanya, B. Alling, and P. Eklund, "Effect of point defects on the electronic density of states of ScN studied by first-principles calculations and implications for thermoelectric properties," *Phys. Rev. B - Condens. Matter Mater. Phys.*, vol. 86, no. 19, pp. 1–7, 2012.
3. S. Acharya *et al.*, "Twinned growth of ScN thin films on lattice-matched GaN substrates," *Mater. Res. Bull.*, vol. 143, no. January, p. 111443, 2021.
4. E. de Prado, J. More-Chevalier, S. Cichoň, and J. Lančok, "Twin domains of ScN (001) films on MgO (001)," *Acta Crystallogr. Sect. A Found. Adv.*, vol. 77, no. a2, pp. C835–C835, 2021.



b)

Figure 1. Results for bi-oriented ScN films. (a) 002 Pole figure and (b) AFM image with phase contrast.

5. S. Chowdhury *et al.*, "Synthesis and study of ScN thin films," pp. 1–13, 2021.
6. J. More-chevalier *et al.*, "Applied Surface Science Correlation between crystallization and oxidation process of ScN films exposed to air," *Appl. Surf. Sci.*, vol. 515, no. December 2019, p. 145968, 2020.